Electronic Supplementary Material (ESI) for Energy & Environmental Science.

Supplementary Materials for

Dopant-free molecular hole transport material that mediates a 20% power conversion efficiency in a perovskite solar cell

Yang Cao[1,4,†], Yunlong Li[2,†], Thomas Morrissey[1,4], Brian Lam[1], Brian O. Patrick[1], David J. Dvorak[4], Zhicheng Xia[1], Timothy L. Kelly[2,*], Curtis P. Berlinguette[1,3,4,*]

correspondence to tim.kelly@usask.ca and cberling@chem.ubc.ca

[†]These authors contributed equally to this work

Synthetic Methods

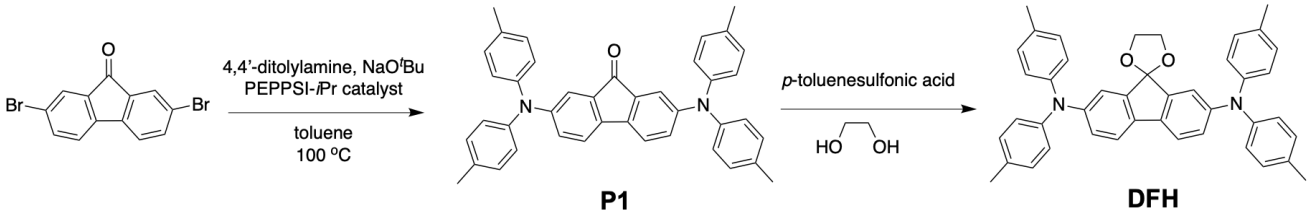

Fig. S1. Synthesis of compounds **P1** and **DFH**.

9-Fluorenone (98.0%, TCI America), 2,7-dibromo-9-fluorenone (98.0%, TCI America), *p*,*p*′-ditolylamine (98.0%, TCI America), ethylene glycol (anhydrous, 99.8%, Sigma-Aldrich), 1,2-propanediol (99.5%, Sigma-Aldrich), *p*-toluenesulfonic acid monohydrate (99%, Sigma-Aldrich), sodium *tert*-butoxide (97%, Sigma-Aldrich) and PEPPSI-IPr catalyst (98%, Sigma-Aldrich) were purchased and directly used without purification. All synthesis steps were performed using anhydrous toluene from a solvent purification system. ^{1}H and ^{13}C{^{1}H} NMR spectra were collected on a Bruker AV400DIR instrument at 25.0 °C with resonance frequencies of 400 MHz and 101 MHz for ^{1}H and ^{13}C nuclei, respectively. Chemical shifts (δ) are reported in parts per million (ppm) using the protio-solvent signals δ 7.26 and 77.0 for chloroform-*d*, δ 5.32 and 53.84 for methylene chloride-d_2 for ^{1}H and ^{13}C NMR spectra, respectively. Standard abbreviations indicating multiplicity are used as follows: s = singlet; d = doublet; dd = doublet of doublets; m = multiplet.

Synthesis of **P1**: The synthesis of **P1** was carried out under N_2 using standard Schlenk techniques. An oven-dried 100 mL two-neck round-bottom flask was connected to the Schlenk line on one neck by via a condenser. A rubber septum was attached to the other neck and the flask was cycled three times between vacuum and nitrogen. 2,7-Dibromo-9-fluorenone (3.38 g, 10.0 mmol), *p*,*p*′-ditolylamine (4.14 g, 21.0 mmol), sodium *tert*-butoxide (2.02 g, 21.0 mmol), PEPPSI™-IPr catalyst (68 mg, 0.10 mmol) and a stir bar were added to the flask and quickly cycled three times. Anhydrous toluene (40 mL) was added via a syringe through the rubber septum which was replaced with a glass stopper under high nitrogen flow. The mixture was stirred for 5 min at room temperature before it was warmed up to 100 °C using an oil bath. After 18 hours, the mixture was poured into 250 mL of methanol and sonicated for 20 min. The dark precipitate was collected via vacuum filtration and washed with 20 mL 0.1M HCl solution, 20 mL deionized water and twice with 20 mL methanol. The purple powder was recrystallized from ethanol/toluene and 5.10 g of pure product was obtained (89 % yield). ^{1}H NMR (400 MHz, chloroform-*d*) δ 7.29 (d, *J* = 2.2 Hz, 2H), 7.19 (d, *J* = 8.2 Hz, 2H), 7.14 – 7.04 (m, 10H), 7.00 (d, *J* = 8.4 Hz, 8H), 2.34 (s, 12H). ^{13}C{^{1}H} NMR (101 MHz, chloroform-*d*) δ 193.90, 148.63, 144.86, 137.53, 135.81, 133.20, 130.20, 127.48, 124.91, 120.23, 118.50, 20.96. HRMS (ESI): *m/z* = 570.2675 [M^+] (calcd for $[C_{41}H_{34}ON_2]^+$: *m/z* = 570.2671).

Synthesis of **DFH**: **P1** (2.00 g, 3.50 mmol), *p*-toluenesulfonic acid monohydrate (50 mg, 0.26 mmol), ethylene glycol (2.00 mL, 32.2 mmol) and a stir bar were added to a round bottom flask which was connected with a condenser via a Dean-Stark trap. The flask was cycled three times between vacuum and N_2 before 40 mL anhydrous toluene was added via syringe. The reaction mixture was heated at 100 °C under N_2 for 2 days before it

was concentrated to around 20 mL under vacuum and poured into 200 mL of methanol. The light yellow precipitate (1.85 g, 84% yield) was collected after vacuum filtration, washing with methanol and drying under high vacuum. After filtration, rinsing and drying under high vacuum 1.77 g (82 % yield) of **DFH** was obtained as a pale white powder.^{1}H NMR (400 MHz, methylene chloride-d_2) δ 7.29 (d, J = 8.2 Hz, 2H), 7.12 – 7.04 (m, 10H), 6.98 (d, J = 8.4 Hz, 8H), 6.94 (dd, J = 8.2, 2.1 Hz, 2H), 4.12 (s, 4H), 2.31 (s, 12H). ^{13}C{^{1}H} NMR (101 MHz, methylene chloride-d_2) δ 148.36, 146.08, 145.87, 133.81, 133.13, 130.41, 125.35, 124.90, 120.37, 119.11, 112.39, 66.16, 21.07. HRMS (ESI): m/z = 614.2937 [M^+] (calcd for $[C_{43}H_{38}O_2N_2]^+$: m/z = 614.2933).

Synthesis of **P2**: P2 without triphenyl amine groups were made to help with peak assignments in ssNMR. 9-Fluorenone (1.26 g, 7.00mmol), *p*-toluenesulfonic acid monohydrate (100 mg, 0.52 mmol), ethylene glycol (4.00 mL, 64.4 mmol) and a stir bar were added to a round bottom flask which was connected with a condenser via a Dean-Stark trap. The reaction mixture was heated at 100 °C under N_2 for 2 days before it was concentrated to around 10 mL under vacuum and poured into 100 mL of methanol. The off-white precipitate (1.22 g, 78% yield) was collected after vacuum filtration, washed with methanol and dried under high vacuum. ^{1}H NMR (400 MHz, chloroform-d) δ 7.58 (dt, J = 7.5, 0.9 Hz, 2H), 7.47 (dt, J = 7.4, 1.0 Hz, 2H), 7.39 (td, J = 7.5, 1.2 Hz, 2H), 7.29 (td, J = 7.5, 1.1 Hz, 2H), 4.43 (s, 4H). ^{13}C{^{1}H} NMR (101 MHz, chloroform-d) δ 144.24, 139.75, 130.30, 128.36, 123.84, 120.04, 112.51, 65.94. HRMS (ESI): m/z = 225.0919 [M+H^+] (calcd for $[C_{43}H_{38}O_2N_2]^+$: m/z = 225.0916).

Cost Analysis

The material cost was calculated using both the lowest available price from the same chemical vendor used in the laboratory gram-scale synthesis, and lowest available price from bulk suppliers (**Table S1** and **S2**).

Table S1. Material Cost to Synthesize **P1**

Chemical	retail price (vendor)	bulk price (vendor)	amount used	retail Cost (bulk cost)
2,7-Dibromo-9-fluorenone	73 USD/25 g (TCI)	118 USD per 100g (Oakwood Chemical)	3.38 g	9.87 USD (<5.24 USD)
Sodium *tert*-butoxide	491 USD/1.5 kg (Sigma)	730 USD per 10 kg (Oakwood Chemical)	2.02 g	0.66 USD (0.15 USD)
p,*p*′-Ditolylamine	70 USD/25 g (TCI)	378 USD per 1000 g (Alichem)	4.14 g	11.59 USD (1.56 USD)
PEPPSI™-IPr catalyst	10,548.83 USD/250 g (Sigma)	10,548.83 USD per 250 g (Sigma)	68 mg	2.87 USD
Toluene	517.67 USD/20 L (Sigma)	517.67 USD per 20 L (Sigma)	40 mL	1.04 USD
P1	**5.10 USD per 1 g**	**2.13 USD per 1 g**	**5.10 g**	**26.03 USD (10.86 USD)**

Table S2. Material cost to synthesize **DFH**

Chemical	retail price (vendor)	bulk price (vendor)	Amount used	retail Cost (bulk cost)
P1	5.10 USD per 1 g	2.13 USD per 1 g	2.00 g	10.20 USD (4.26 USD)
Ethylene glycol	341.74 USD per 6 L (Sigma)	150 USD per 10 kg (abcr.de)	2.00 mL	0.11 USD (0.03 USD)
Toluene	517.67 USD per 20 L (Sigma)	517.67 USD per 20 L (Sigma)	40 mL	1.04 USD
p-Toluenesulfonic acid monohydrate	101.16 per 2.5 kg	101.16 per 2.5 kg	50 mg	0.002 USD
DFH	**6.41 USD per 1g**	**3.02 USD per 1g**	**1.77 g**	**11.35 USD (5.35 USD)**

Characterization of Compounds

Solution UV-Vis absorption spectra were collected on a Cary 5000 spectrophotometer (**Fig. S2A**). Solution photoluminescence spectra were recorded with a Cary Eclipse fluorimeter (**Fig. S2B**). All solution samples were measured in a 1 cm quartz cell at room temperature in HPLC grade DCM. The concentrations of the DCM solutions of analytes for UV-Vis and photoluminescence measurements were 2×10^{-5} mol·L^{-1} and 1×10^{-5} mol·L^{-1}, respectively. Solid-state absorptance (%A) was measured on a Cary 7000 spectrophotometer by subtracting reflection (%R) and transmission (%T) from incident light (**Fig. S3**).

Differential pulse voltammetry (DPV) data was recorded with a CHI660D potentiostat at room temperature using a platinum wire counter electrode and a platinum working electrode (**Fig. S4**). Ag/AgCl in saturated KCl was used as the reference electrode and was calibrated versus the normal hydrogen electrode (NHE) by the addition of ferrocene. A 0.1 M *n*-NBu_4PF_6 electrolyte solution in DCM was used for all HTMs. DPV data were acquired for 0.5 mM solutions of compounds at a scan rate of 50 mV·s^{-1}. Differential scanning calorimetry (DSC) data was recorded using a Netzsch DSC Polyma 214 calorimeter under a N_2 purge flow at a scan rate of 10 K·min^{-1}.

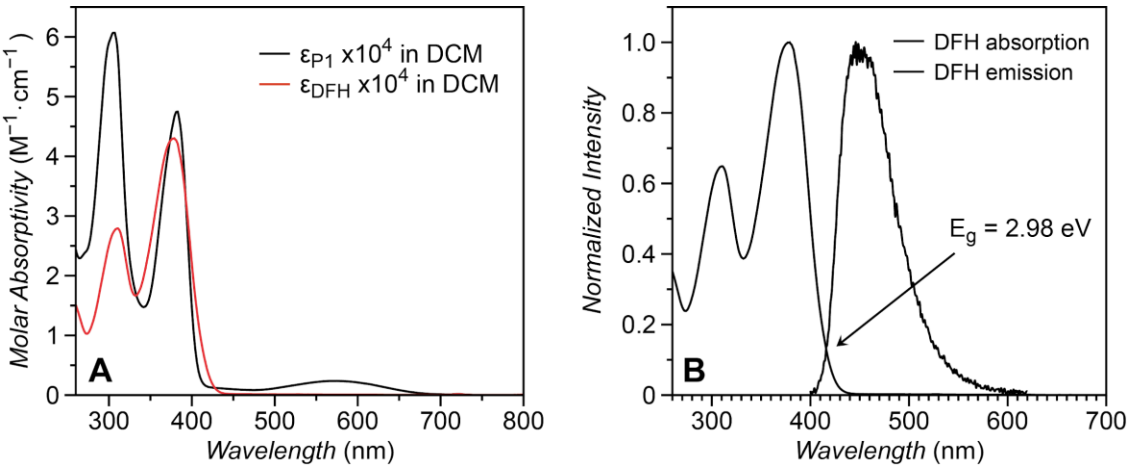

Fig. S2. (a) Molar absorptivity of **P1** and **DFH** in dichloromethane. (b) Normalized absorption and emission spectra of **DFH**.

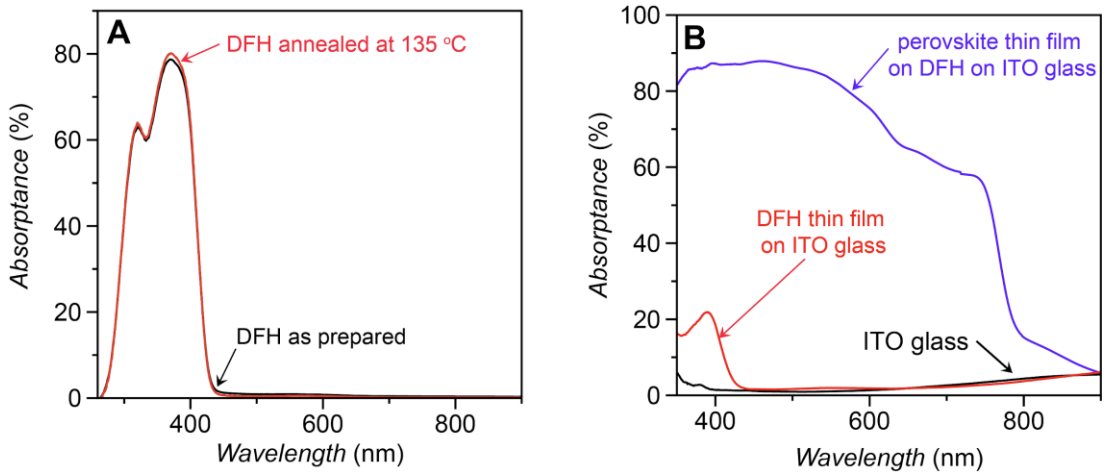

Fig. S3. (A) UV-Vis spectra of spin-coated (60 mg/mL in chlorobenzene, 3000 rpm for 30s) solid state thin films of **DFH**, unheated and annealed at 135 °C for 20 mins. (B) UV-Vis spectra of the ITO glass substrate, DFH on ITO glass substrate (spin-coated at 6000 rpm for 30s from a 15 mg/mL solution in chlorobenzene, and annealed at 135 °C for 20 mins), and perovskite thin film (coated with the same method used for the fabrication of full devices) on aforementioned DFH on ITO glass substrate.

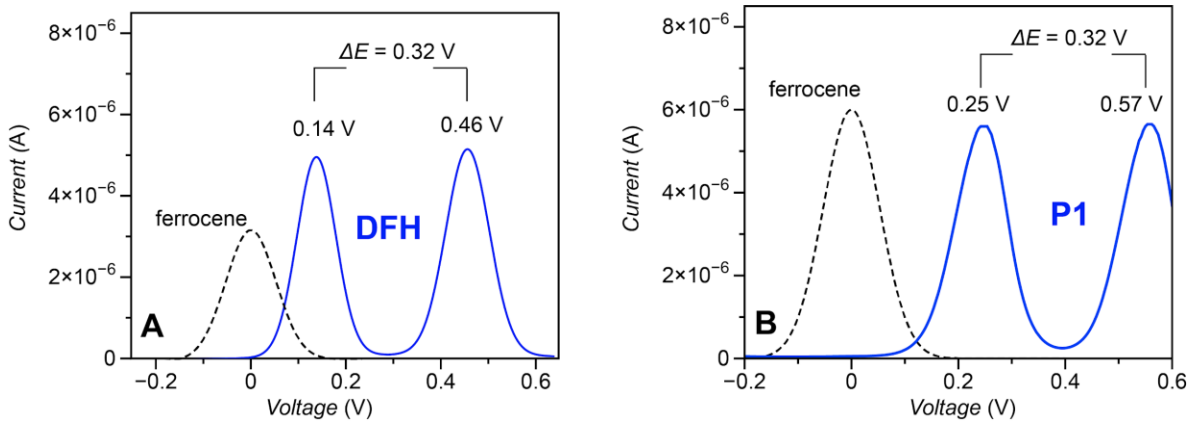

Fig. S4. Differential pulse voltammetry (DPV) of (A) **DFH** and (B) **P1** in dichloromethane showing the voltage of two strongly coupled oxidation events relative to the Fc^{+}/FcH redox couple.

Table S3. Summary of the Optical, Electrochemical and Electrical Properties of **DFH**.

λ_{abs} (nm)	λ_{em} (nm)	$E_{1/2}$ (V)	E_{gap} (eV)	E_{HOMO} (eV)
370	450	0.14	2.98	-5.27

Half-wave redox potentials ($E_{1/2}$) in DCM are relative to that of ferrocene ($E_{FcH/Fc+}$ = 630 mV vs NHE). E_{gap} was estimated from the intersection of normalized absorption and emission spectra. E_{HOMO} (eV) = - 4.5 - $E_{1/2}$ (V vs NHE).

X-ray Crystallography

Single crystal X-ray crystallography was performed using a Bruker APEX II area detector diffractometer. Single colourless tablet-shaped crystals of **DFH** were recrystallized from a mixture of toluene and ethanol by slow diffusion. Suitable crystals were selected and mounted on a mylar loop. Data were measured using MoK_{α} radiation (microfocus sealed X-ray tube, 50 kV, 0.99 mA). The structure was solved with the **SHELXT** [1] structure solution program using the Intrinsic Phasing solution method and by using **Olex2** [2] as the graphical interface. The diffraction pattern indexing, unit cell refinement, data reduction, scaling and absorption corrections were performed using **SAINT** (Bruker, V8.38A, after 2013). Multi-Scan absorption correction was performed using **SADABS**-2016/2 (Bruker, 2016/2). All non-hydrogen atoms were refined anisotropically. Hydrogen atom positions were calculated geometrically and refined using the riding model. **DFH**: The maximum resolution that was achieved was $Q = 30.629^{\circ}$ (0.70 Å). The structure was solved and the space group *P*-1 (# 2) determined by the **XT** structure solution program using Intrinsic Phasing and refined by Least Squares using version 2017/1 of **XL**. There is a small amount of disorder in the 1,3-dioxolane moiety that was modelled in two orientations.

Table S4. Summary of the Structure Parameters of **DFH** Single Crystal.

Chemical Formula	$C_{43}H_{38}N_2O_2$
Density of Crystal, $D_{calc.}$ ($g \cdot cm^{-3}$)	1.220
Formula Weight (g/mol)	614.75
Colour, Shape and Size of Crystal (mm^3)	colourless, tablet, 0.41×0.24×0.12
Crystal System, Space Group	triclinic, *P*-1
a, b, c (Å)	10.5358(10), 12.5714(12), 15.0206(14)
α, β, γ (°)	101.715(2), 107.958(2), 109.766(2)
V ($Å^3$)	1672.8(3)
Numbers of molecules in unit cell, *Z*	2

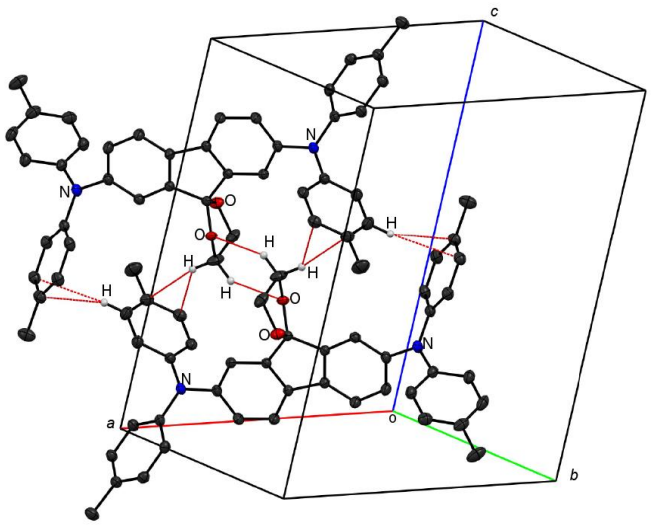

Fig. S5. ORTEP thermal ellipsoid presentation of the CH···O hydrogen bonding and C-H···π interactions between dimeric **DFH** molecules. Non-interacting hydrogens have been omitted for clarity.

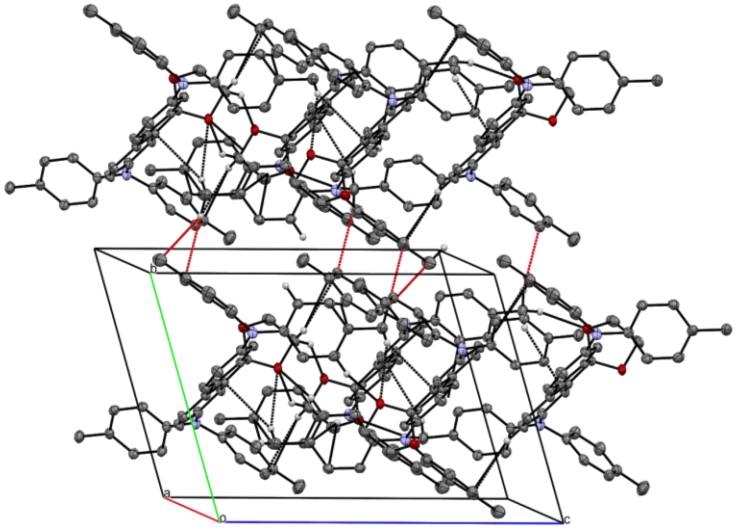

Fig. S6. ORTEP thermal ellipsoid presentation of the C-H···π interactions between adjacent (010) face of the **DFH** crystal lattice. Non-interacting hydrogens have been omitted for clarity.

Density Functional Theory Calculations

DFT calculations were carried out using the Gaussian 09 Rev-D.01 software [3]. Molecular properties such as molecular energies, HOMO levels and electrostatic surface potential mapping were modeled using long-range corrected ω-B97XD functional [4] with 6-311G** basis set. The reorganization energy λ (0.021 Hartree or 0.57 eV) of **DFH** was calculated the following equation:

$$\lambda = E^{+*} - E - E^{+} + E^{*},$$

where E is the energy of the neutral state with optimized neutral geometry (-1921.2364792 Hartree), E^{+*} is the energy of the cationic state with the optimized neutral-state geometry (-1921.0093504 Hartree), E^{+} is the energy of the cationic state with optimized cationic geometry (-1921.0194704 Hartree) and E^{*} is the energy of the neutral state with the optimized cationic geometry (-1921.225525 Hartree). All four energies are calculated in vacuum. According to literature [5], the reorganization energy of Spiro-OMeTAD was calculated to be 0.31 eV using the same long-range corrected functional.

The electronic interaction energy ($E_{\text{HTM-HTM}}$) between **DFH** dimers with crystallographic atomic coordinates was calculated using counterpoises and corrected for basis set superposition error (BSSE)[6]. The following two different basis sets were used.

$E_{\text{HTM-HTM}}$ = -25.16 kcal/mol or -105 kJ/mol (6-31+G** for interacting H, 6-31G** for everything else)

$E_{\text{HTM-HTM}}$ = -26.19 kcal/mol or -110 kJ/mol (6-311+G** for interacting H, 6-311G** for everything else)

X-ray Diffraction

Powder and thin film X-ray diffraction experiments were performed on a Rigaku SmartLab X-ray diffractometer using CuK_{α} radiation. A Bragg-Brentano θ-θ geometry was used to probe powder samples annealed at different temperatures. The scanning range was from 5° to 25°, with 0.02° per step. The thin film was characterized using 2θ scans using parallel-beam grazing-incidence X-ray diffraction (GIXD). The HTM film was spin-coated on a glass substrate and annealed at 150 °C on a hotplate until formation of visible spherulites on the thin film. The scanning range was from 5° to 60°, with 0.04° per step, the incidence angle was 0.7°.

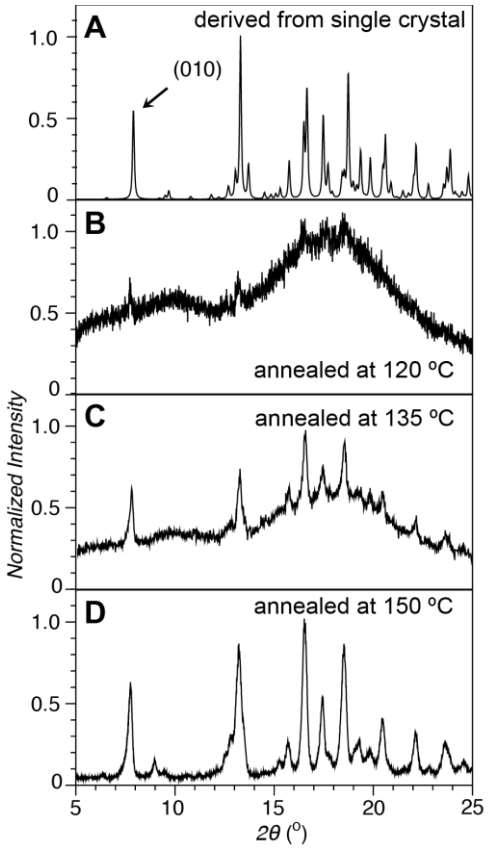

Fig. S7. The powder XRD spectra of **DFH** derived from its crystal structure (A) and measured XRD spectra of **DFH** annealed at 120 °C (B), 135 °C (C) and 150 °C (D).

Solid-State NMR

^{13}C CP-MAS NMR spectra with high power proton decoupling were collected on a 400MHz Bruker solid state DRX spectrometer. Sample was spinning at 6 kHz at magical angle. Ramped pulse on ^{13}C frequency was used for cross polarization with a contact time of 4ms for all experiments. Relaxation delay was set to be 5 seconds, and acquisition time 50ms. Data were processed with a 20 Hz line broadening exponential decay function. Chemical shifts (δ, in ppm) were referenced with adamantane $^{13}CH_2$ signal at 29.5ppm. All experiments are performed at room temperature. Peak assignments were carried out using an analogue without the ditolyamine groups (**fig. S7**).

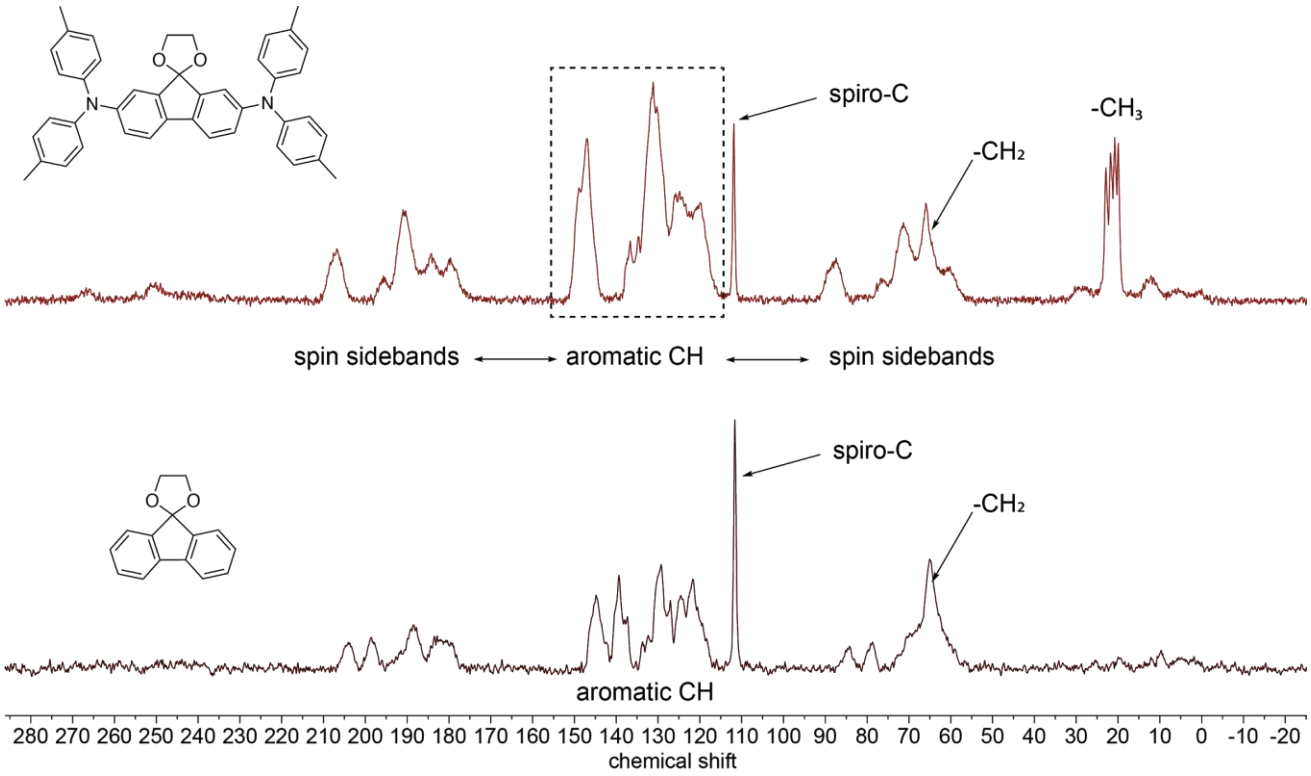

Fig. S8. The assignment of peaks and spin-sidebands of crystalline solid-state **DFH** and control **P2**.

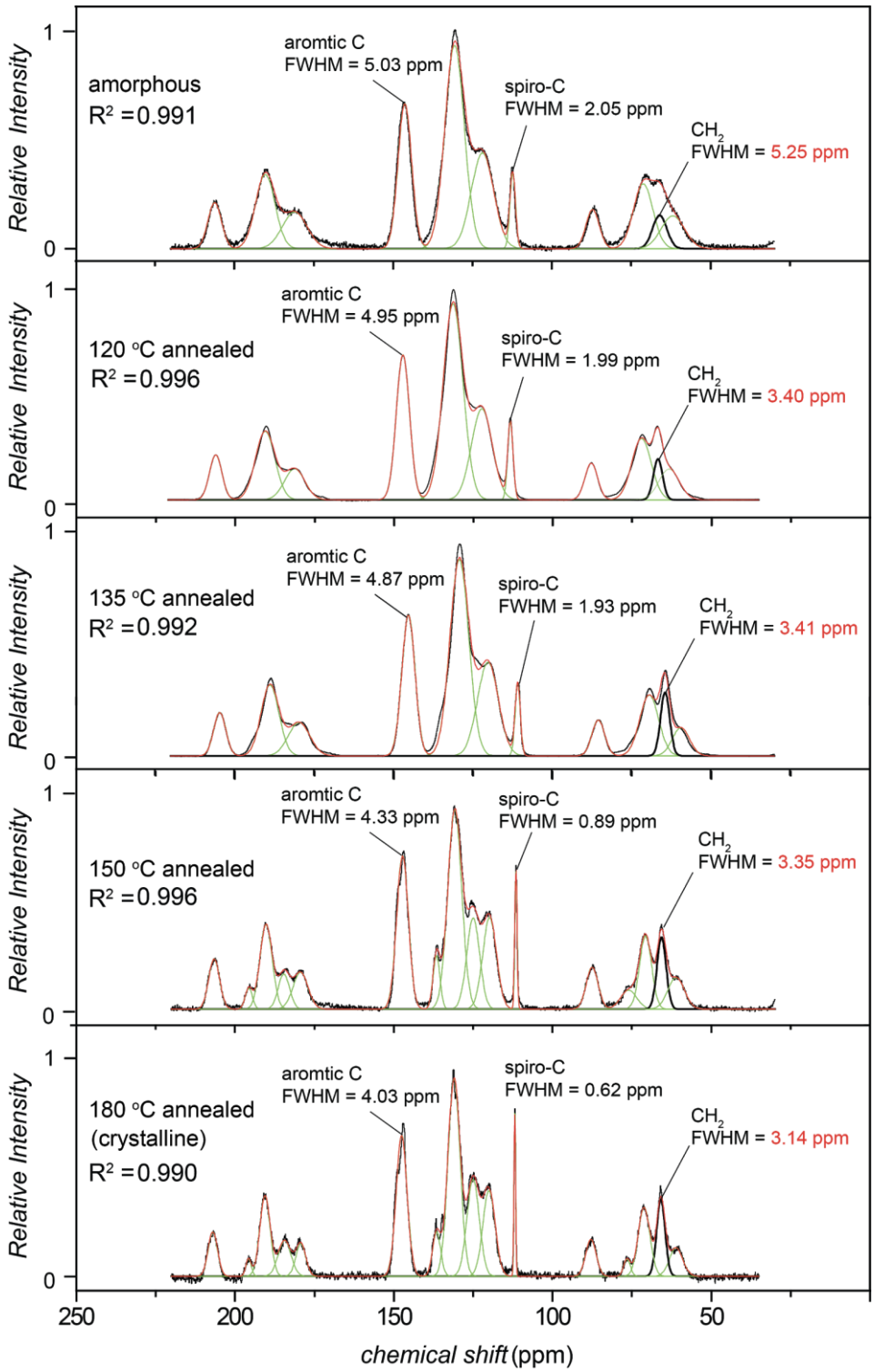

Fig. S9. Fitted high power CP-MAS NMR spectra of **DFH** between 220 ppm and 30 ppm, the methylene peak was highlighted in black.

Mobility and Conductivity Measurements

The hole mobility of **DFH** was measured on hole-only devices (ITO/MoO_3/HTM/Au) using the space-charge-limited current (SCLC) method. The hole mobility was determined by fitting the quadratic region of the *I*/*V* curve to the Mott-Gurney law.

$$J_d = \frac{9\varepsilon\varepsilon_0\mu V_b^2}{8L^3},$$

where L is the thickness of the **DFH** layer (here $L \approx 40$ nm), the relative dielectric constant of **DFH** (ε) was assumed to be 3, ε_0 is the vacuum permittivity, and V_b is the applied voltage.

Conductivity values were obtained using measurements on four different thin film devices on the same conductive ITO substrate with a spin-coated HTM layer and four sputtered Au contacts (ITO/HTM/Au). The HTM bulk resistance R was calculated by subtracting the non-HTM resistance from the total device resistance, assuming that the resistance of HTM thin films obtained with different spin speeds (1200 rpm and 3000 rpm) is directly proportional to their thickness (around 210 nm for 1200 rpm and 150 nm for 3000 rpm, respectively), and that the non-HTM resistance including Au-HTM contact resistance remains the same. The HTM conductivity was obtained using $\sigma = d \cdot R^{-1} \cdot A^{-1}$, where d is the thickness of the film, and A is the effective area (12 mm^2). The HTM films were annealed prior to the Au deposition since Au-HTM contact resistance reduces significantly with heating.

Table S5. Hole conductivities and mobilities for **DFH** and selected HTMs.

Condition	μ_h ($\times 10^{-3}$ $cm^2 \cdot V^{-1} \cdot s^{-1}$)[C]	*Conductivity* ($\times 10^{-3}$ $mS \cdot cm^{-1}$)[B]
DFH (as-prepared)	0.9	3.5
DFH (annealed @ 135 °C)	1.1	7.4
KR321	0.26	-
PTAA (doped with Li^+)	0.43	-
spiro-OMeTAD (doped with Li^+)	0.69	117

(A) Hole mobility was measured using the space-charge-limited-current (SCLC) method on hole-only devices (ITO/MoO_3/HTM/Au). (B) Conductivity was calculated using $\sigma = d \cdot R^{-1} \cdot A^{-1}$, where R *is* the film resistance measured on ITO/HTM/Au, A is the effective area (12 mm^2) and, d is the thickness of the HTM thin film. For each condition, two different d each in four devices were measured in order to subtract the contact resistances which are independance to d. (C) Thickness ~ 40 nm.

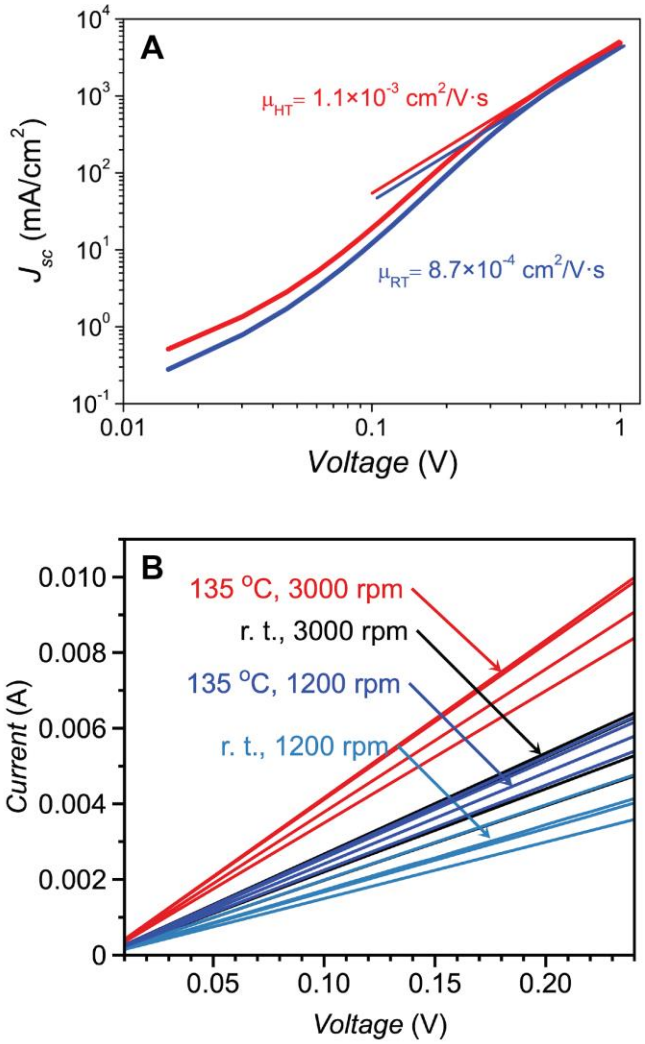

Fig. S10. (A) Hole mobility measurements of **DFH** in hole-only devices. The device configuration is ITO/MoO_3/HTM/Au, where the HTM layer was either stored at room temperature after spin-coating or annealed at 135 °C. (B) Traces of conductivity measurements of **DFH**.

Fluorescence Lifetime Measurement

Experiments were carried out using a customized laser system provided by the LASIR facility at the University of British Columbia. Pulsed (10 Hz) 532 nm laser was used to excite (prompt) perovskite samples on various substrates and the emitted photons were probed by a Hamamatsu dynamic range streak camera (C7700). The device architecture is glass/HTM/perovskite/PMMA.

Solar Cell Fabrication and Characterization

Methylammonium iodide (MAI) and formamidinium iodide (FAI) were synthesized by the reaction of methylamine and formamidine with hydroiodic acid, respectively, as previously reported. ITO coated glass substrates were obtained from Xin Yan Technology Ltd (2.5 cm × 2.5 cm, R_s = 20 Ω/□). PbI_2 (99.9985%), C_{60} (99.5%), bathocuproine (BCP) (98%) and silver (Ag) (99.99%) were purchased from Fisher Scientific, Nano-C, Fisher Scientific, and Kurt J. Lesker, respectively. All materials were used without any further purification.

ITO-coated glass substrates were cleaned by 20 min sonication in each of detergent (extran 300, 2%), deionized water, acetone and isopropanol. After drying in a stream of nitrogen, a 15 min ultraviolet-ozone treatment was carried out immediately prior to the deposition of the hole transport layer (HTL). **DFH** was dissolved in chlorobenzene (10, 15, or 20 mg/mL) and deposited on the ITO substrate by spin-coating (6000 rpm for 30 s). The films were then annealed at various temperatures for 20 min on a hotplate in ambient air. PTAA HTLs were deposited by spin coating from a 1.5 mg/mL toluene solution, as reported previously[45]. An $MAPbI_3$ perovskite precursor solution (1.2 M) was prepared by mixing MAI and PbI_2 (1:1 molar ratio) in anhydrous mixed solvent (4:1 DMF/DMSO). A solution of FAI and $PbCl_2$ was also prepared at the same concentration using the same solvent mixture. The two solutions were combined in a 9:1 ratio (MA:FA, v/v) to produce the final perovskite precursor solution. Perovskite layers were deposited by dropping the precursor solution onto the substrate, and after spinning at 4000 rpm for 7 s, dropping anhydrous chlorobenzene (120 μL) onto the center of the substrate. The substrate was spun for a further 30 s at 4000 rpm without pause. The transparent yellow films obtained after spin coating were heated at 35 °C for 20 min, after which they became black. The films were further annealed at 85 °C for 10 min. To complete the device stack, C_{60} (40 nm), BCP (8 nm) and Ag (100 nm) were sequentially deposited by thermal evaporation at a base pressure of 1×10^{-6} mbar.

Current-voltage curves of perovskite solar cells and hole-only devices were recorded with a Keithley 2400 source-measure unit. Devices were measured in the glovebox (H_2O < 1 ppm, O_2 < 0.1 ppm) using a 450 W Class AAA solar simulator equipped with a AM1.5G filter (Sol3A, Oriel Instruments). Before measuring, a standard silicon reference cell (91150V, Oriel Instruments) was used to set the light intensity to 1 sun. During the measurement, the cell was covered by a non-reflective metal mask with an aperture of 0.0708 cm^2. Incident photon to current (IPCE) measurements were performed in air using a QE-PV-SI system (Oriel Instruments) consisting of a 300 W Xe arc lamp, monochromator, chopper, lock-in amplifier and certified silicon reference cell, operating at a 30 Hz beam-chopping frequency. Scanning Electron Microscopy (SEM) images were acquired on either a FEI Helios NanoLab 650 dual beam SEM at 5 kV and 50 pA or a Hitachi SU8010 microscope at 3 kV and 10 pA using a through-lens detector in secondary electron mode.

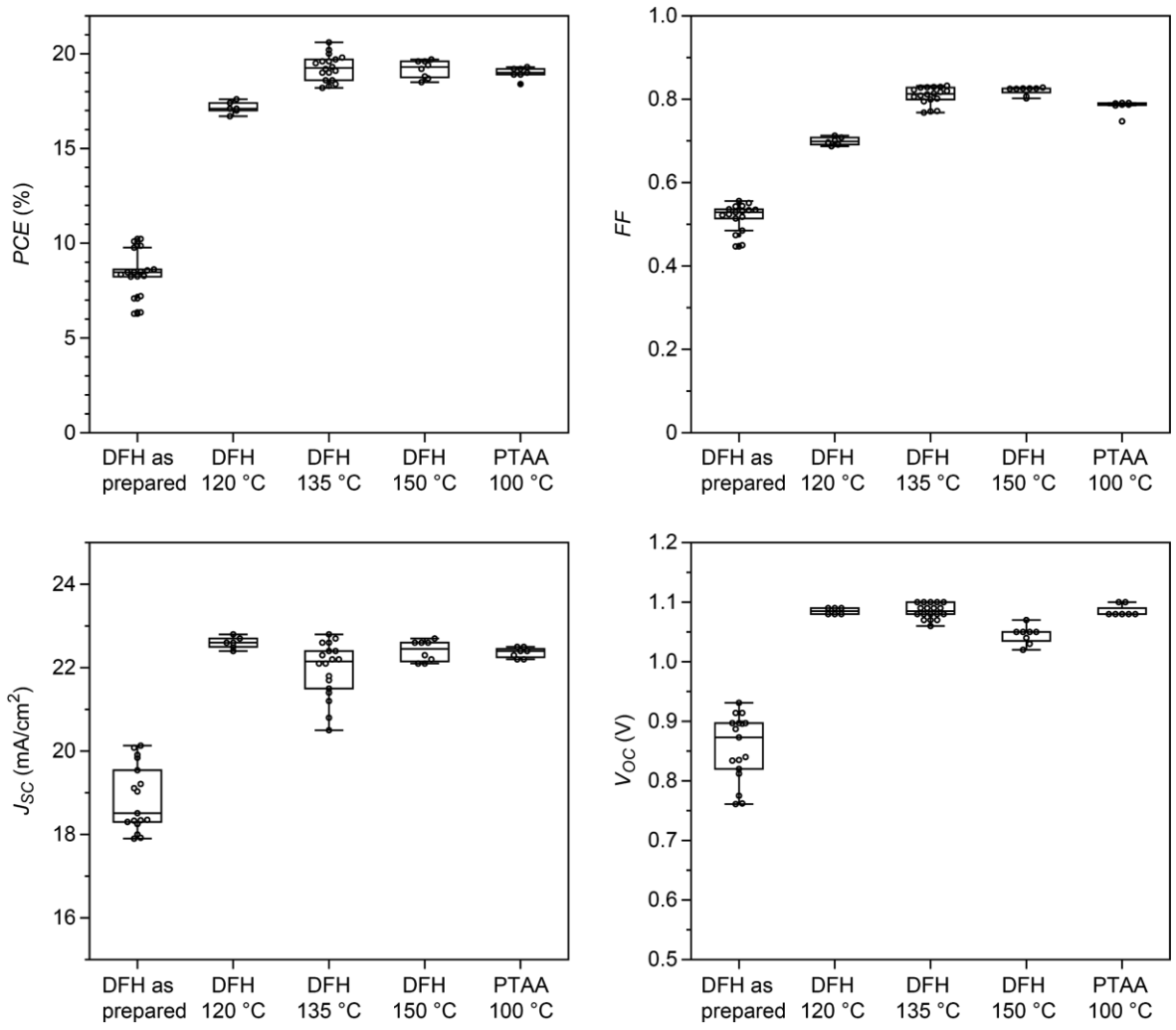

Fig. S11. Device performance statistics for PSCs with different hole transport layers obtained by reverse $J-V$ scans. Sample sizes are 17, 6, 18, 8 and 7 for devices with as prepared DFH, 120 °C annealed DFH, 135 °C annealed DFH, 150 °C annealed DFH and 100 °C annealed PTAA as hole transport layers. PTAA was annealed at 100 °C according to device optimization in literature.[7]

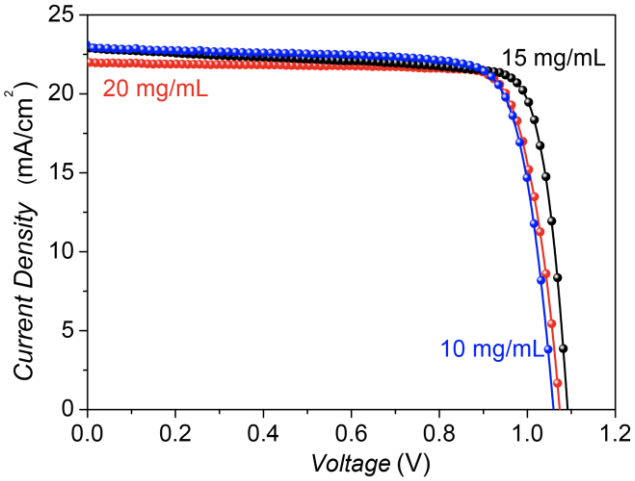

Fig. S12. *J-V* curves of PSCs with varying thickness of **DFH** layers, illustrating the effect of **DFH** thickness on PSC performance.

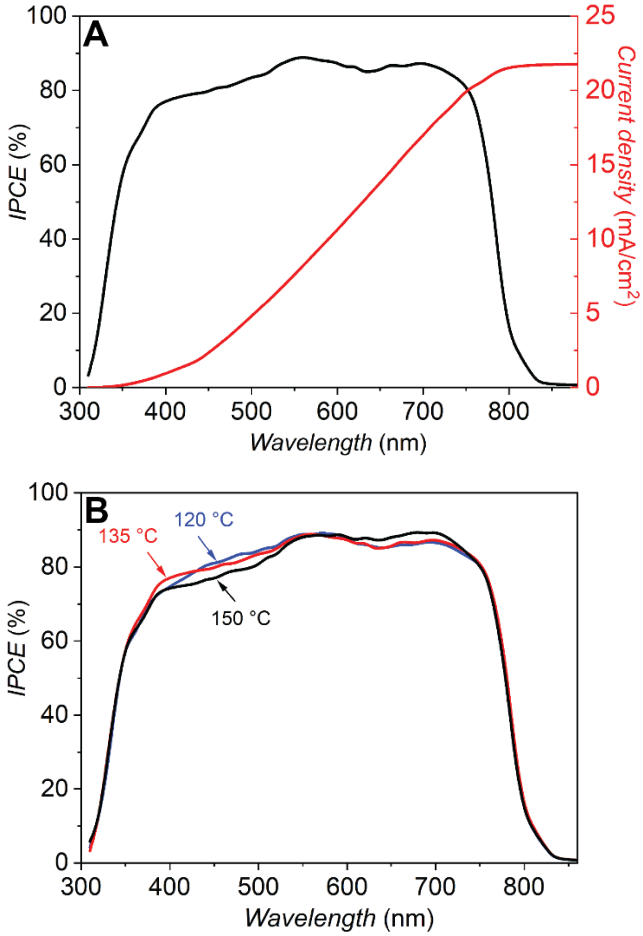

Fig. S13. (A) IPCE spectra and integral current density of a PSC with a **DFH** HTL annealed at 135 °; (B) IPCE spectra of PSCs with **DFH** HTL annealed at 120 °C, 135 °C and 150 °C.

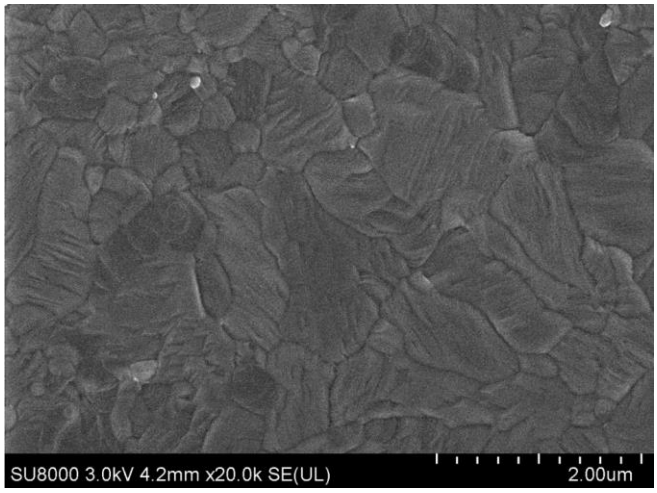

Fig. S14. SEM images of perovskite layers grown on a thin film of 135 °C annealed **DFH**. The scale bar is 2 μm.

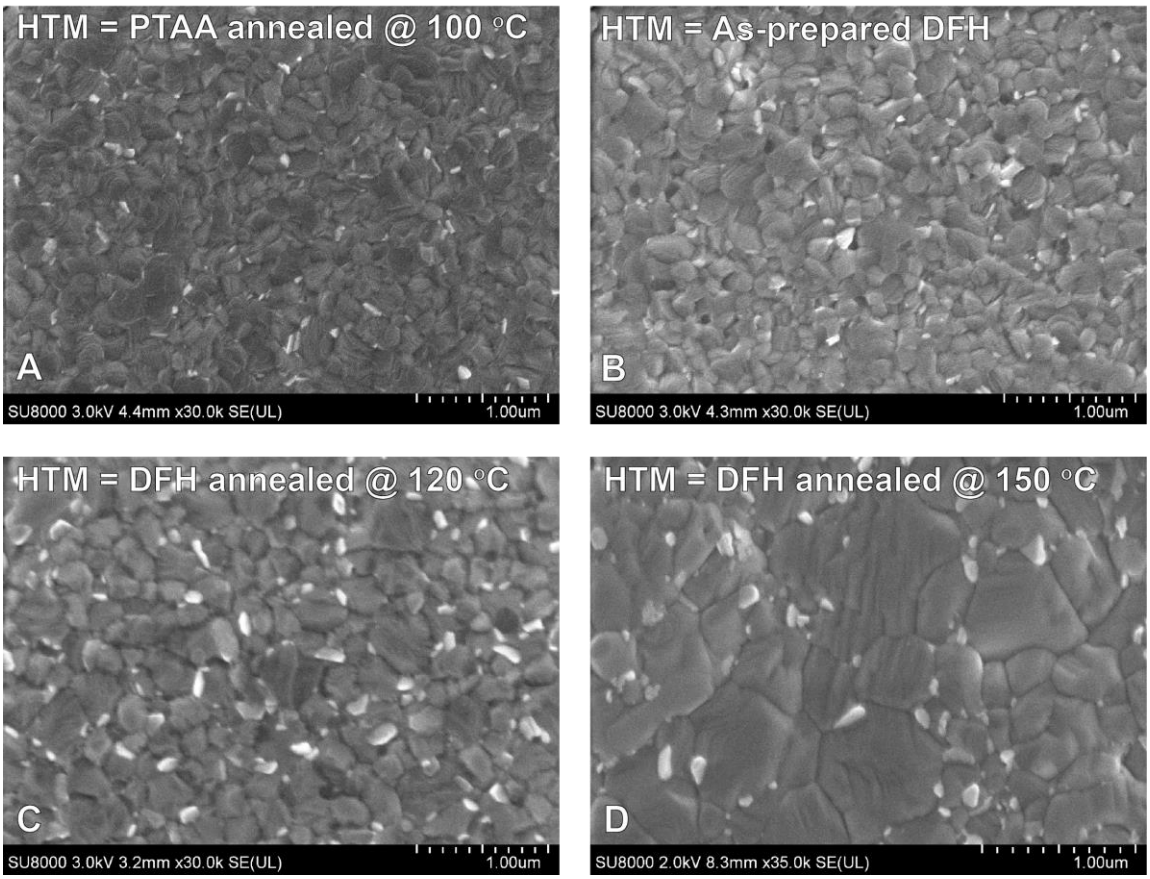

Fig. S15. SEM images of perovskite layers grown on thin films of (A) 100 °C annealed PTAA (B) as-prepared and unheated DFH and (C) 120 °C annealed **DFH** and (D) 135 °C annealed **DFH**. The scale bars are 1 μm.

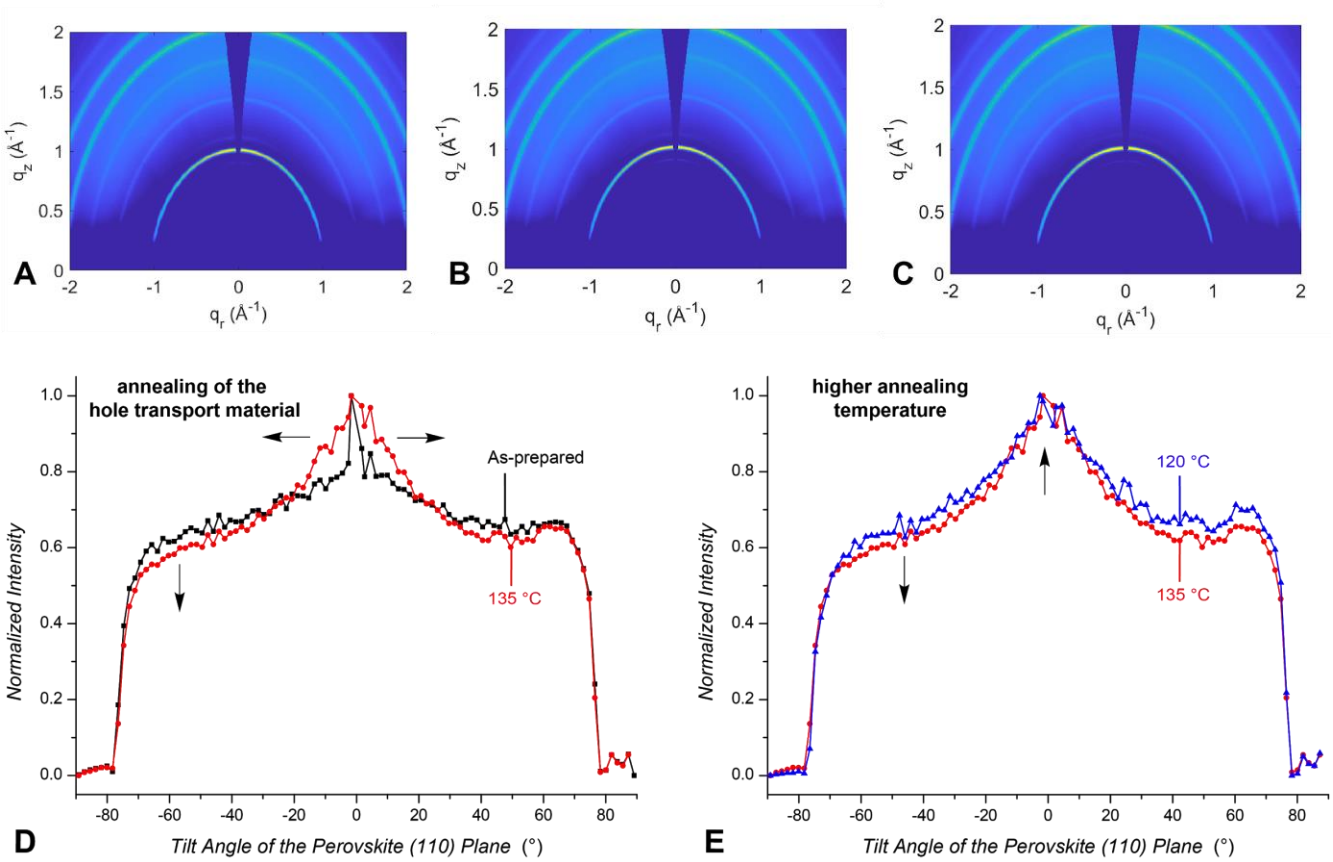

Fig. S16. GIXD patterns of perovskite layers grown on **DFH** thin films (A) as-prepared (B) annealed at 120 °C, and (C) annealed at 135 °C. Radially integrated intensity plots of the GIXRD patterns along the q = 1.0106 $Å^{-1}$ ring assigned to the (110) plane showing the differences between the perovskite layers grown on (D) as-prepared and 135 °C annealed **DFH**, and (E) 120 °C and 135 °C annealed **DFH**.

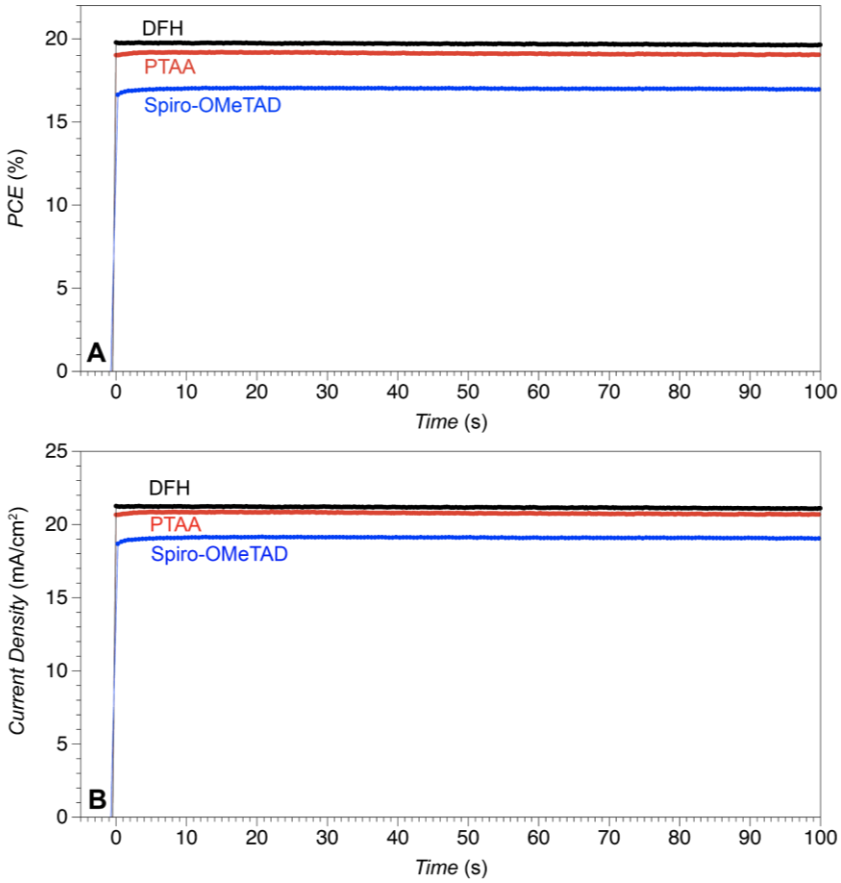

Fig. S17. Stabilized (A) *PCE* and (B) current density of PSCs with 135°C annealed hole transport layers measured at the maximum power points every 0.25 seconds, the potentials for DFH, PTAA and Spiro-OMeTAD are 0.93 V, 0.92 V and 0.89 V, respectively.

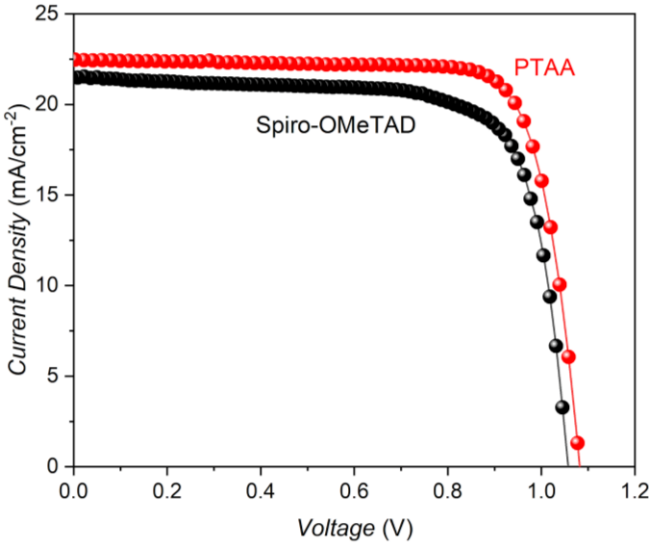

Fig.S18. Reverse J−V scans of champion PSCs with PTAA and Spiro-OMeTAD hole transport layers.

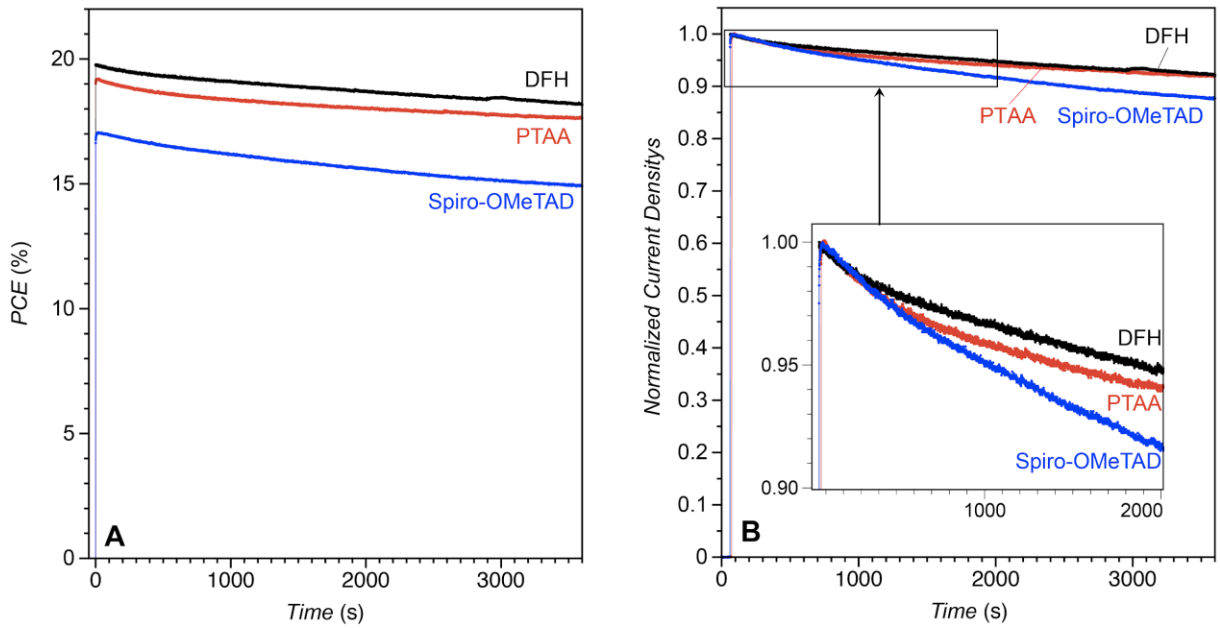

Fig. S19. Operational stability in terms of the decay of (A) *PCE* and (B) normalized current density of perovskite solar cells under 1-sun condition loaded with a constant voltage of their initial maximum power points (0.93 V, 0.92 V and 0.89 V for **DFH**, PTAA and Spiro-OMeTAD, respectively).

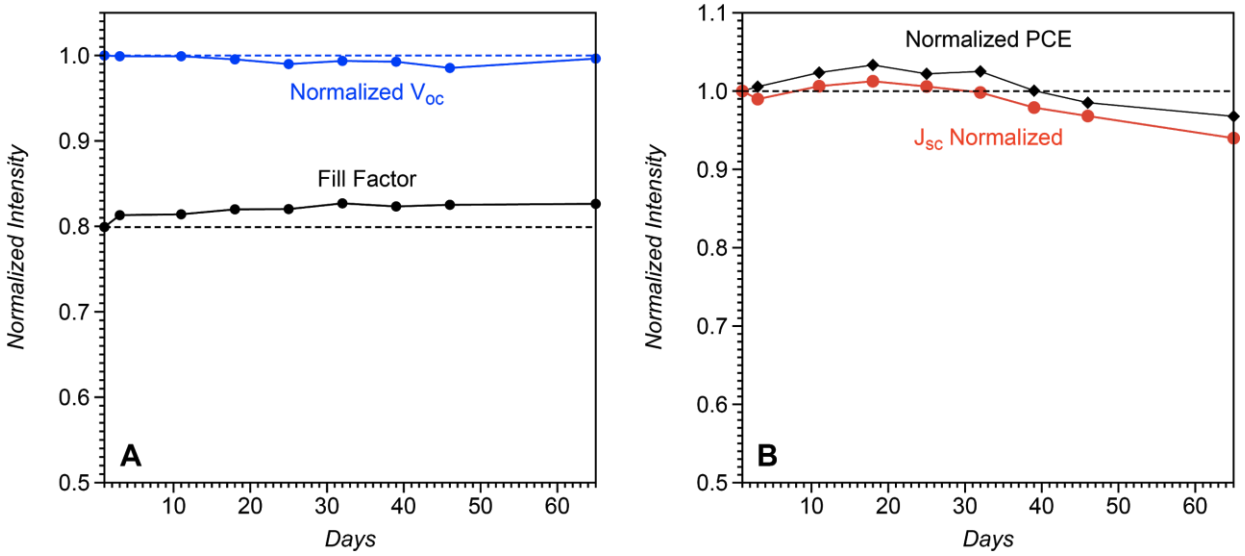

Fig. S20. Storage stability of a PSC device with 135 °C annealed **DFH**, under an inert atmosphere. Dashed lines indicate data collected on day 1. Initial *PCE* = 19.3%, V_{oc} = 1.09 V; *FF* = 0.79.

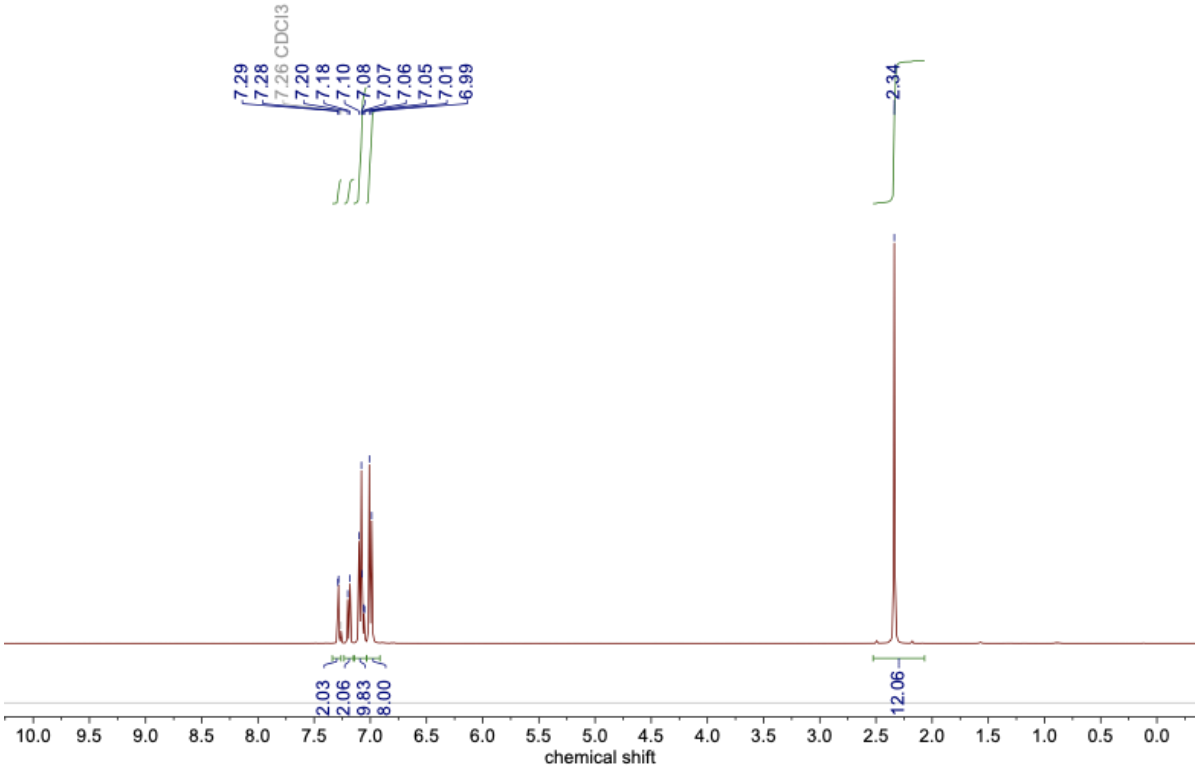

Fig. NMR1. ^{1}H NMR spectrum of **P1** in $CDCl_{3.}$

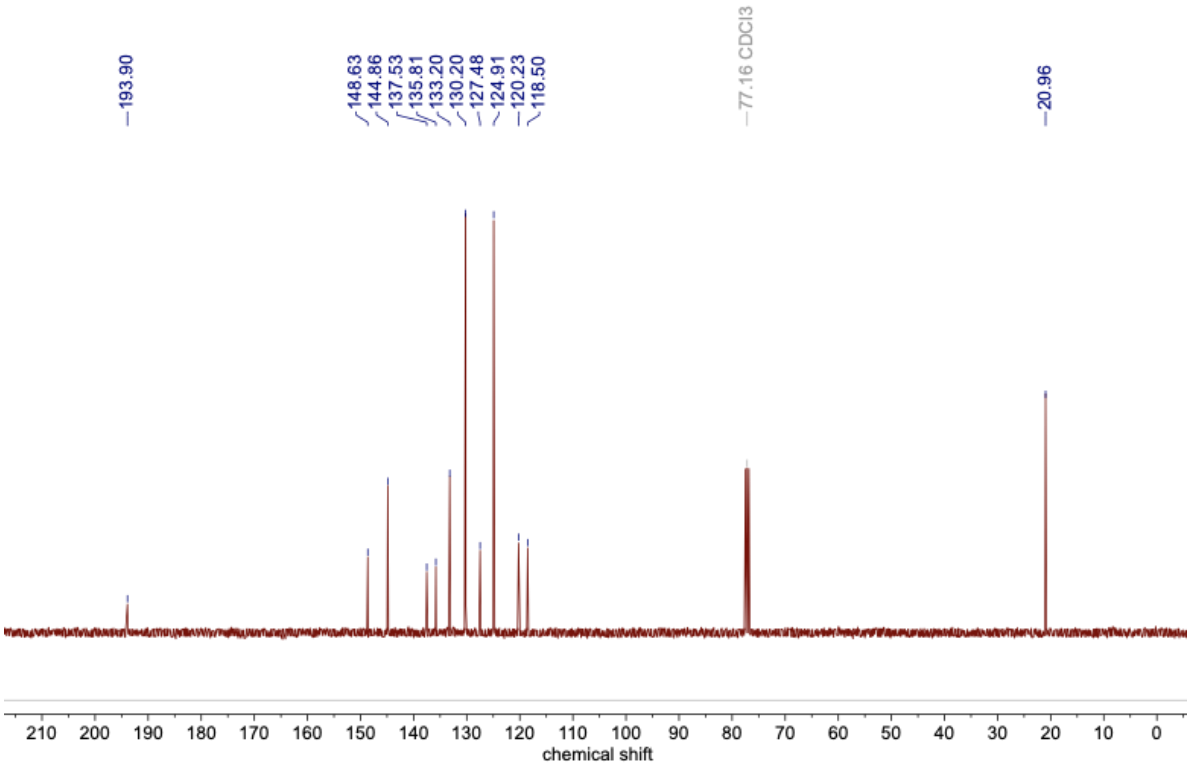

Fig. NMR2.$^{13}C\{^{1}H\}$ NMR spectrum of **P1** in $CDCl_3$

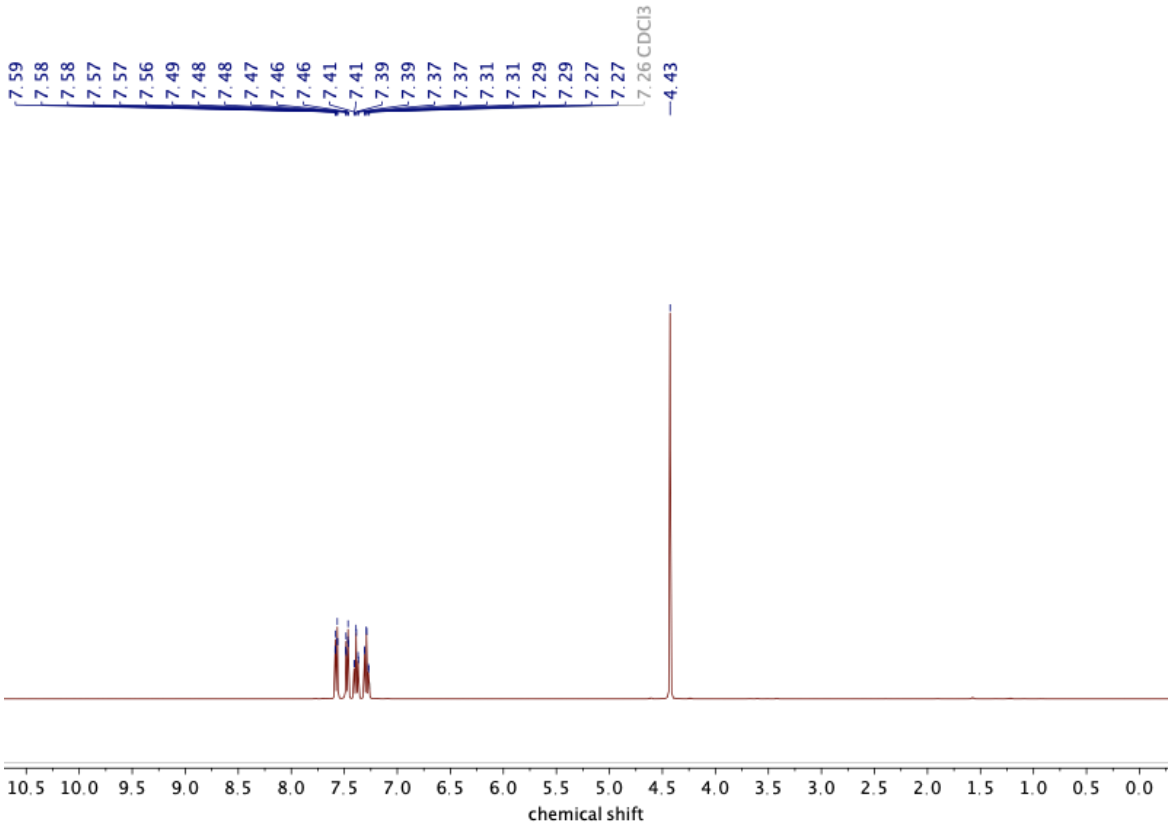

Fig. NMR3. ^{1}H NMR spectrum of **P2** in CD_2Cl_2.

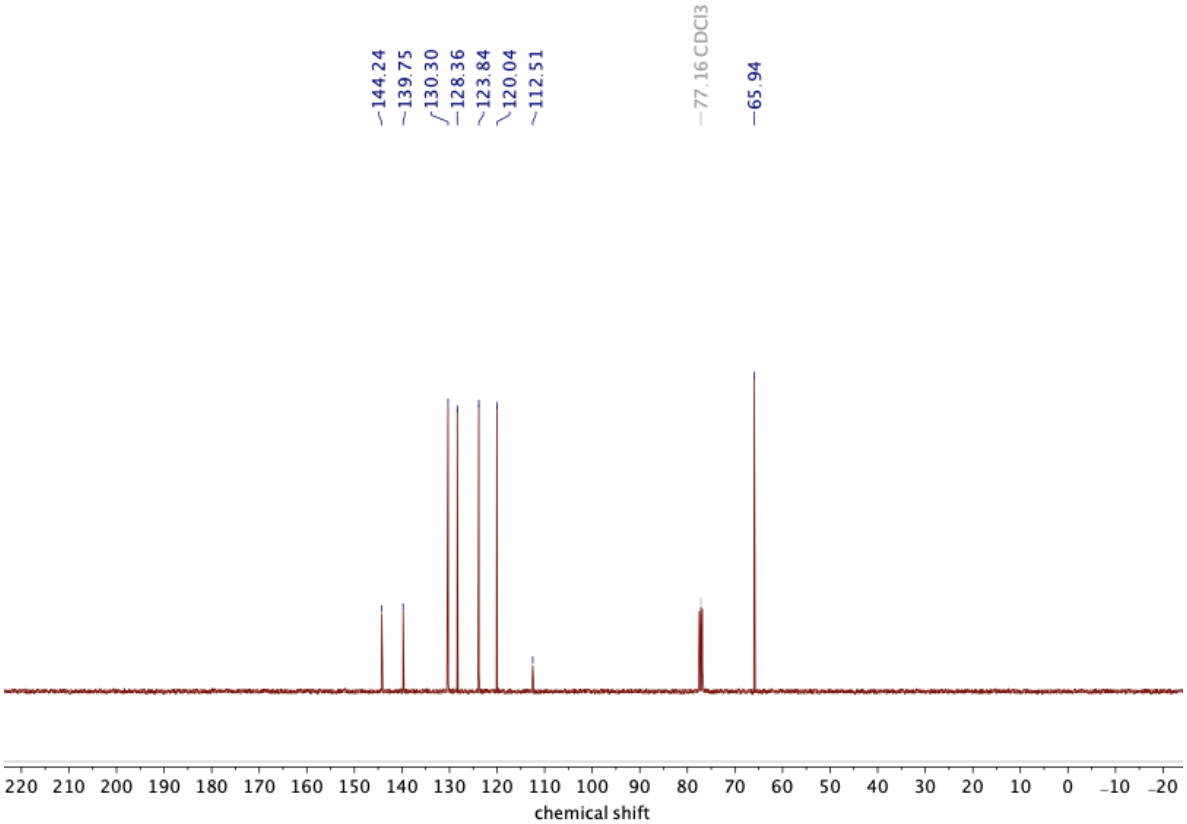

Fig. NMR4. $^{13}C\{^{1}H\}$ NMR spectrum of **P2** in CD_2Cl_2.

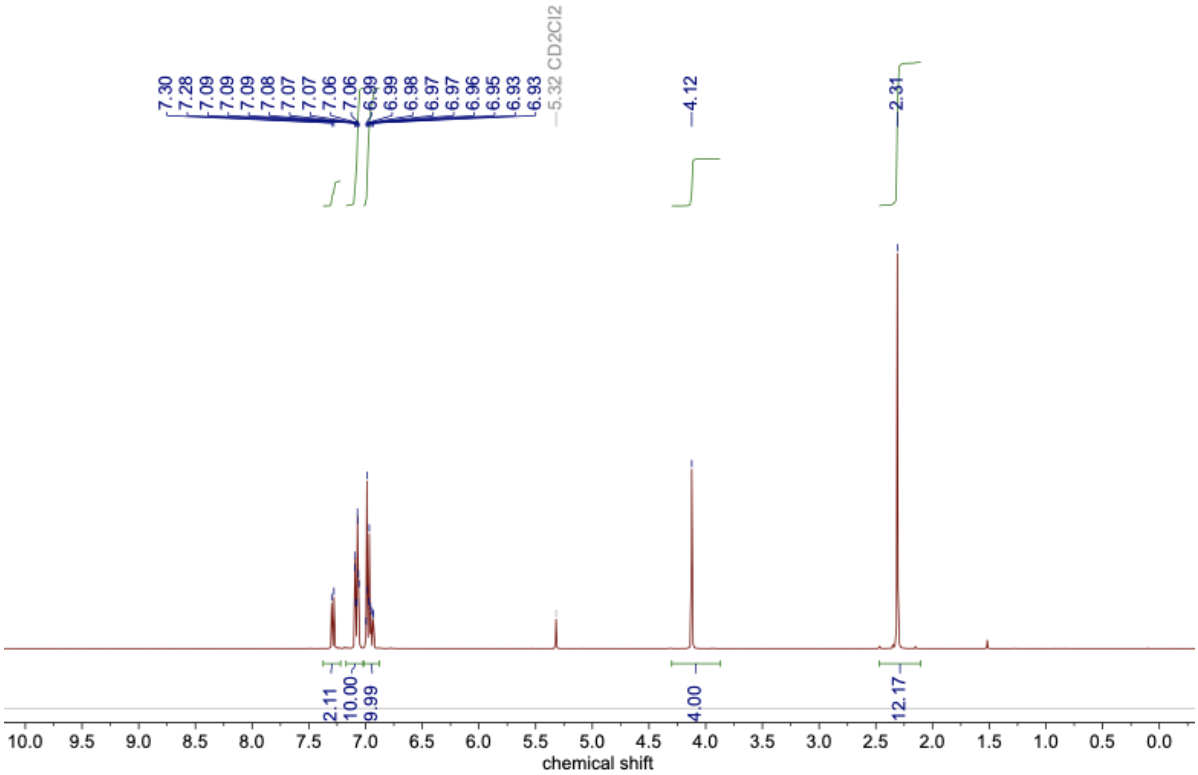

Fig. NMR5. ^{1}H NMR spectrum of **DFH** in CD_2Cl_2.

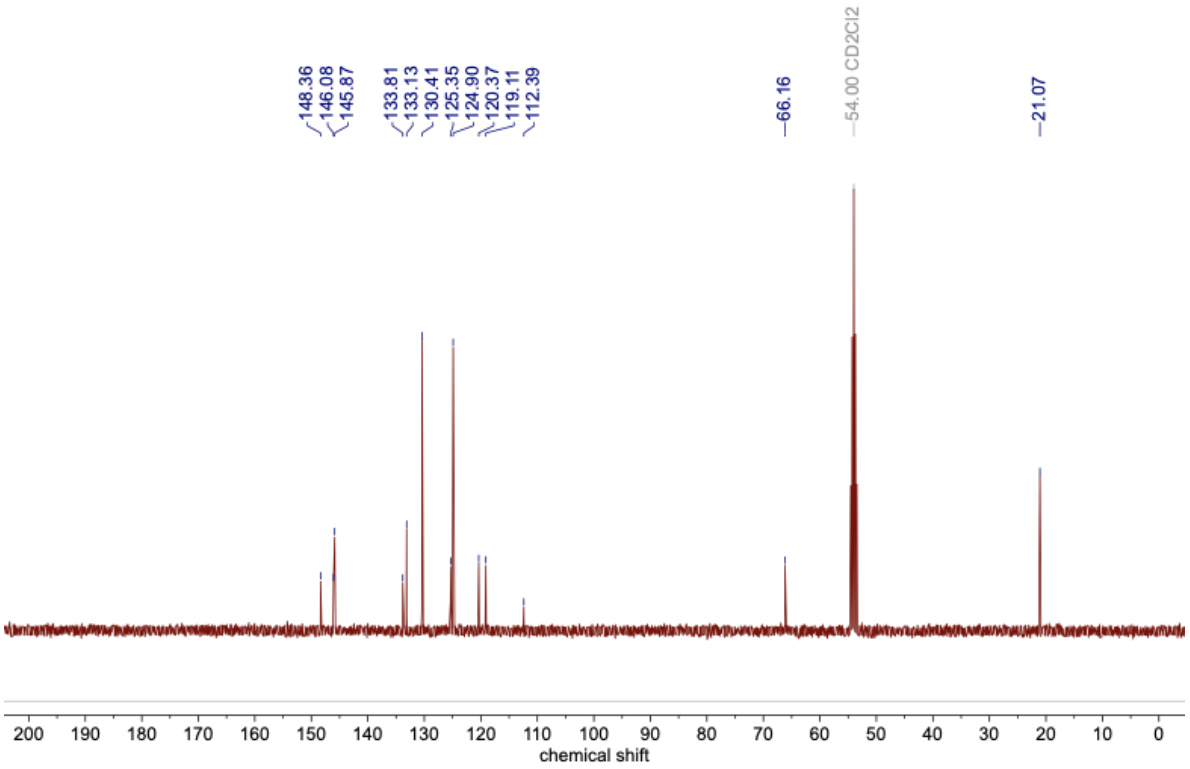

Fig. NMR6. ^{13}C{^{1}H} NMR spectrum of **DFH** in CD_2Cl_2.

References :

1 G. M. Sheldrick, *Acta Crystallogr. A*, 2015, **71**, 3–8.
2 O. V. Dolomanov, L. J. Bourhis, R. J. Gildea, J. A. K. Howard and H. Puschmann, *J. Appl. Crystallogr.*, 2009, **42**, 339–341.
3 M. J. Frisch, G. W. Trucks, H. B. Schlegel, G. E. Scuseria, M. A. Robb, J. R. Cheeseman, G. Scalmani, V. Barone, G. A. Petersson, H. Nakatsuji, X. Li, M. Caricato, A. Marenich, J. Bloino, B. G. Janesko, R. Gomperts, B. Mennucci, H. P. Hratchian, J. V. Ortiz, A. F. Izmaylov, J. L. Sonnenberg, D. Williams-Young, F. Ding, F. Lipparini, F. Egidi, J. Goings, B. Peng, A. Petrone, T. Henderson, D. Ranasinghe, V. G. Zakrzewski, J. Gao, N. Rega, G. Zheng, W. Liang, M. Hada, M. Ehara, K. Toyota, R. Fukuda, J. Hasegawa, M. Ishida, T. Nakajima, Y. Honda, O. Kitao, H. Nakai, T. Vreven, K. Throssell, J. A. Montgomery, J. E. Peralta, F. Ogliaro, M. Bearpark, J. J. Heyd, E. Brothers, K. N. Kudin, V. N. Staroverov, T. Keith, R. Kobayashi, J. Normand, K. Raghavachari, A. Rendell, J. C. Burant, S. S. Iyengar, J. Tomasi, M. Cossi, J. M. Millam, M. Klene, C. Adamo, R. Cammi, J. W. Ochterski, R. L. Martin, K. Morokuma, O. Farkas, J. B. Foresman, and D. J. Fox, Gaussian, Inc. , Wallingford CT, 2016., *Gaussian 09 Rev-D.01*, .
4 J.-D. Chai and M. Head-Gordon, *Phys. Chem. Chem. Phys.*, 2008, **10**, 6615–6620.
5 Y. Li, H. Li, C. Zhong, G. Sini and J.-L. Brédas, *npj Flexible Electronics*, 2017, **1**, 2.
6 J. B. Foresman and Æ. Frisch., *Exploring Chemistry with Electronic Structure Methods*, 3rd ed. (Gaussian, Inc., Wallingford, CT, 2015).
7 M. Stolterfoht, C. M. Wolff, Y. Amir, A. Paulke, L. Perdigón-Toro, P. Caprioglio and D. Neher, *Energy Environ. Sci.*, 2017, **10**, 1530–1539.